A MICROSCOPIC STUDY ON SHEARING MECHANISM OF SOILS

MECANISME DE CISAILLEMENT DES SOLS

МИКРОСКОПИЧЕСКИЕ ИССЛЕДОВАНИЯ МЕХАНИЗМА СДВИГА В ГРУНТАХ

S. MURAYAMA, Professor, Kyoto University

H. MATSUOKA, Research Associate, Kyoto University, Japan

SYNOPSIS. In order to analyze the macroscopic stress-strain relation of granular soils, the shearing mechanism was studied from a microscopic point of view. For this purpose, a special shearing test was carried out using aluminium rods with various diameters or similar rods made of photoelastic material to simulate granular mass in a two-dimensional state. Stress-strain relations of soils including stress ratio-strain increment ratio relations were analyzed from the microscopic consideration and the results were verified by experiments using sands or clays

INTRODUCTION

The granular nature of soils found in sands and clays should be one of the most essential properties of soils. Therefore, the shearing mechanism of granular soils has been investigated from a microscopic viewpoint by applying direct shear tests with rod masses. The rod masses, which consist of horizontally piled cylindrical aluminium rods (ϕ1.6, 3mm; ϕ3, 5, 9mm) or similar rods made of photoelastic material (ϕ6.2, 10mm), are two-dimensional models of granular materials. On these experiments, the angle of contact plane between particles θ, the interparticle force f and the frictional angle between particles ϕ_μ are adopted as essential factors which control the shearing resistance of soils. The concept of "the frequency distribution of θ and its variation during shear" is introduced to represent the macroscopic shearing resistance and dilatancy character.

MICROSCOPIC ANALYSIS OF STRESS-STRAIN RELATIONS

The shearing resistance and dilatancy of granular soils are studied from the following microscopic consideration. The mobilized particles which slide relatively along the potential sliding plane are shown in Fig. 1. At the i-th contact point the interparticle force is called f_i, the angle of contact plane, θ_i. The angle of contact plane is defined as the angle between the contact plane of particles and the potential sliding plane. The frictional angle ϕ_μ is assumed to be constant at each mobilized contact point along the sliding plane. Then, the shear stress-normal stress ratio (τ/σ_N) on the potential sliding plane can be generally represented by the following equation.

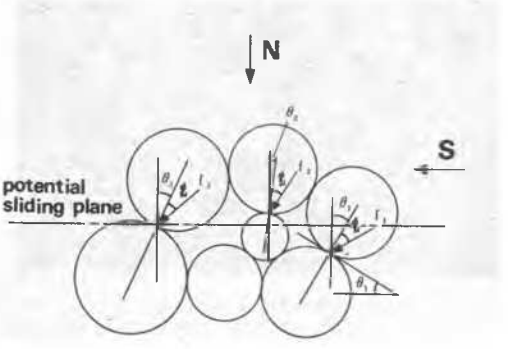

Fig. 1 The angle of contact plane between particles θ_i, the interparticle force f_i and the frictional angle between particles ϕ_μ

$$\frac{\tau}{\sigma_N} = \frac{S}{N} = \frac{\sum_{i=1}^{n} f_i \cdot \sin(\theta_i + \phi_\mu)}{\sum_{i=1}^{n} f_i \cdot \cos(\theta_i + \phi_\mu)} \qquad (1)$$

where n: number of contact points of mobilized particles, τ, S: shear stress and shear force along the potential sliding plane i.e. along the $(\tau/\sigma_N)_{max}$-plane respectively, σ_N, N: normal stress and normal force on the same plane respectively. Subdividing the overall domain of θ;($-90^\circ \sim +90^\circ$) into the small sections of equal interval $\Delta\theta$ whose medium value is θ_j, and introducing F_j as the sum of the interparticle forces f_i in each subdivided section θ_j, Eq. (1) is represented as follows.

$$\frac{\tau}{\sigma_N} = \frac{\sum_{j=1}^{m} F_j \cdot \sin(\theta_j + \phi_\mu)}{\sum_{j=1}^{m} F_j \cdot \cos(\theta_j + \phi_\mu)} \qquad (2)$$

where m: number of the subdivided sections of $\Delta\theta$. The number of contact points between particles in a subdivided section θ_j (j = 1~m) means the frequency number N_j of the following θ.

$$\theta_j - \Delta\theta/2 < \theta < \theta_j + \Delta\theta/2$$

$$F_j = \sum f_i = \frac{\sum f_i}{N_j} \cdot N_j = \bar{f}_j \cdot N_j \qquad (3)$$

From Eq. (3), F_j is represented as the product of average interparticle force $\bar{f}_j$ and N_j. In order to measure F_j, direct shear tests were performed using rods made of photoelastic material. From such experimental result as shown in Photo. 1, the relation between F_j and N_j before and during shear was obtained at the first approximation as follows.

$$F_j \fallingdotseq C \cdot N_j \quad (C: \text{const.}) \qquad (4)$$

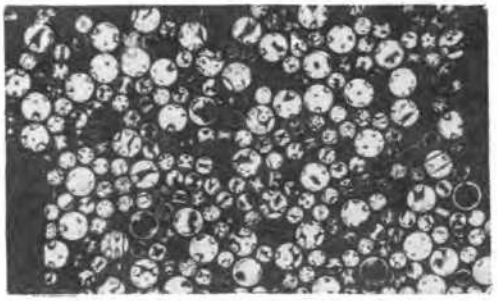

Photo. 1 Isochromatic lines of photoelastic rod mass at the residual strength state

Substituting Eq. (4) into Eq. (2), we get:

$$\frac{\tau}{\sigma_N} = \frac{\sum_{j=1}^{m} N_j \cdot \sin(\theta_j + \phi_\mu)}{\sum_{j=1}^{m} N_j \cdot \cos(\theta_j + \phi_\mu)} \qquad (5)$$

Replacing the discrete function N_j by the continuous function $N(\theta)$, Eq. (5) is written in a integral form as follows.

$$\frac{\tau}{\sigma_N} = \frac{\int_{-\frac{\pi}{2}}^{\frac{\pi}{2}} N(\theta) \cdot \sin(\theta + \phi_\mu) \cdot d\theta}{\int_{-\frac{\pi}{2}}^{\frac{\pi}{2}} N(\theta) \cdot \cos(\theta + \phi_\mu) \cdot d\theta} \qquad (6)$$

If the function $N(\theta)$ is given, the shearing resistance (τ/σ_N) can be obtained by integrating the above equation.

Therefore, the variation of $N(\theta)$ during shear has been investigated by the measurement of the angles of contact planes on the potential sliding plane in the ordinary photographs taken during direct shear tests using rod

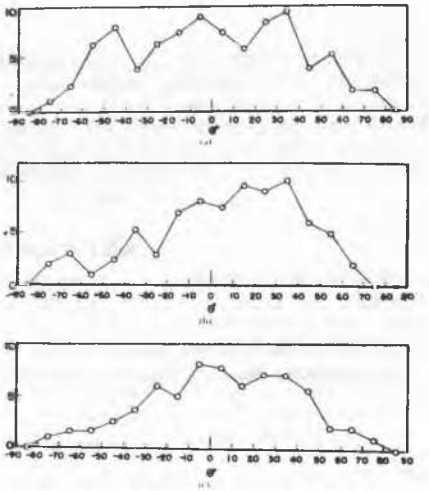

Fig. 2 Frequency distribution of θ of aluminium rod mass
(a) before shear (b) at the peak strength (c) at the residual strength

masses, steel balls and actual sands. Fixed patterns of $N(\theta)$ during shear were observed in the case of dense samples as shown in Fig. 2; namely, (a) the symmetrical distribution at the initial state. (b) the rightwards inclined distribution at the peak strength which means that many angles of contact planes tend to the positive side of θ. The more the distribution tends to the right, the more the mass resists against shear. (c) the symmetrical distribution appears again at the residual strength. From Fig. 2 $N(\theta)$ may be approximated to be a trapezoidal or triangular distribution as shown in Fig. 3.

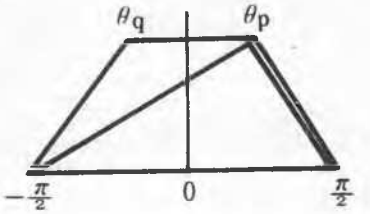

Fig. 3 Trapezoidal and triangular frequency distribution of θ

By using such approximation, the shear stress-normal stress ratio (τ/σ_N) can be calculated from Eq. (6) as follows: in the case of the trapezoidal distribution,

$$\frac{\tau}{\sigma_N} = \frac{(\pi/2-\theta_p)\sin(\theta_q+\phi_\mu)+(\theta_q+\pi/2)\sin(\theta_p+\phi_\mu)-(\theta_p+\theta_q)\cos\phi_\mu}{(\pi/2-\theta_p)\cos(\theta_q+\phi_\mu)+(\theta_q+\pi/2)\cos(\theta_p+\phi_\mu)+(\theta_p+\theta_q)\sin\phi_\mu} \qquad (7)$$

in the case of the triangular distribution where θ_p equals θ_q,

$$\frac{\tau}{\sigma_N} = \frac{\pi\cdot\sin(\theta_p + \phi_\mu) - 2\theta_p\cdot\cos\phi_\mu}{\pi\cdot\cos(\theta_p + \phi_\mu) + 2\theta_p\cdot\sin\phi_\mu} \qquad (8)$$

Since θ_q does not approach too near to $-\pi/2$, the value of τ/σ_N is not affected so sensitively by the selection of the above two distributions. Therefore, the triangular distribution was adopted because of its simpler form. Under this adoption, the average value of θ: $\bar{\theta}$ is represented by

$$\bar{\theta} = \int_{-\frac{\pi}{2}}^{\frac{\pi}{2}} N(\theta)\cdot\theta\cdot d\theta \Big/ \int_{-\frac{\pi}{2}}^{\frac{\pi}{2}} N(\theta)\cdot d\theta = \theta_p/3$$

From the above equation and Eq. (8), the relation between τ/σ_N and $\bar{\theta}$ can be calculated. This calculated result can be approximately represented by the linear relation in a certain range of $\bar{\theta}$ as shown in Fig. 4. Therefore, this relation is expressed with a parameter ϕ_μ as follows.

$$\frac{\tau}{\sigma_N} = \lambda\cdot\bar{\theta} + \mu \qquad (9)$$

where $\mu = \tan\phi_\mu$, and λ is the gradient of this straight line in Fig. 4, which is measured as $1.4 \sim 1.5$.

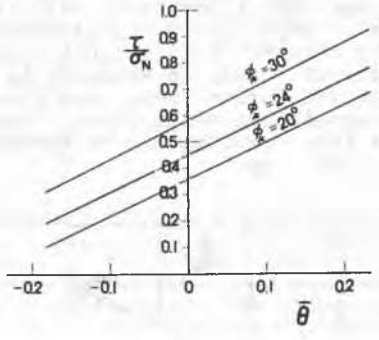

Fig. 4 Relationship between τ/σ_N and $\bar{\theta}$ with parameter ϕ_μ

Fig. 5 shows the microscopic mechanism of dilatancy of granular soils. If n' particles exist in the normal direction to the potential sliding plane, the whole length L and its increment ΔL due to the decrement of the angle of contact plane $\Delta\theta_i$ can be represented as follows.

$$L = \sum_{i=1}^{n'-1} (r_i + r_{i+1})\cdot\cos\theta_i + (r_1 + r_{n'}) \qquad (10)$$

$$\Delta L = \sum_{i=1}^{n'-1} \Delta l_i = \sum_{i=1}^{n'-1} (r_i + r_{i+1})\cdot\sin\theta_i\cdot\Delta\theta_i \qquad (11)$$

where r_i is the radius of the i-th particle and Δl_i is the increment of the normal displacement shown in Fig. 5. In the case of uniform shear deformation such as simple shear deformation, it is considered that the variation of $N(\theta)$ in the normal direction caused by the shear deformation must be the same

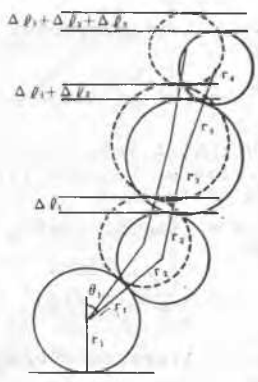

Fig. 5 Microscopic mechanism of dilatancy

pattern as shown in Fig. 2. Since r_i in Eqs. (10) and (11) has no functional relation to θ_i, an average operation is performed by describing the average value of (r_i+r_{i+1}) as $\bar{d}$ and that of θ_i as $\bar{\theta}$. Namely,

$$L = (n' - 1)\cdot\bar{d}\cdot\cos\bar{\theta} + \bar{d} \fallingdotseq (n' - 1)\cdot\bar{d}\cdot\cos\bar{\theta} \qquad (12)$$

$$\Delta L = (n' - 1)\cdot\bar{d}\cdot\sin\bar{\theta}\cdot\Delta\bar{\theta} \qquad (13)$$

If L at the initial state before shearing is denoted as L_o, the following equation is obtained from Eqs. (12) and (13).

$$(\Delta L/L_o)/\Delta\bar{\theta} = \sin\bar{\theta}/\cos\bar{\theta}_o \qquad (14)$$

where $\bar{\theta}_o$ is $\bar{\theta}$ immediately after the beginning of shearing. Since it may be assumed that $(\Delta L/L_o)$ corresponds to the increment of the normal strain of rod mass $-\Delta\varepsilon_N$ (possitive ε_N means compression) and that $\Delta\bar{\theta}$ corresponds to the increment of the shear strain $\Delta\gamma$, we get:

$$-\frac{\Delta L/L_o}{\Delta\bar{\theta}} \fallingdotseq \frac{\Delta\varepsilon_N}{\Delta\gamma} \fallingdotseq \frac{d\varepsilon_N}{d\bar{\theta}} = \frac{\sin\bar{\theta}}{\cos\bar{\theta}_o} \qquad (15)$$

Integrating Eq. (15) and appling the condition (i.e. $\varepsilon_N=0$ when $\bar{\theta}=\bar{\theta}_o$), the following equation is obtained for the case that τ/σ_N is less than the peak strength.

$$\varepsilon_N = \frac{\cos\bar{\theta} - \cos\bar{\theta}_o}{\cos\bar{\theta}_o} \qquad (16)$$

After τ/σ_N exceeds the peak strength, $\bar{\theta}$ decreases with the increase of γ. But if the similar treatment as used above is applied to $\bar{\theta}$ after the peak, ε_N can be calculated as follows.

$$\varepsilon_N = \frac{2\cos\bar{\theta}_p - \cos\bar{\theta} - \cos\bar{\theta}_o}{\cos\bar{\theta}_o} \qquad (17)$$

where $\bar{\theta}_p$ is $\bar{\theta}$ at the peak strength. Substituting Eq. (15) into Eq. (9), the relation

between τ/σ_N and $d\varepsilon_N/d\gamma$ is given as follows.

$$\frac{\tau}{\sigma_N} = \lambda\cdot\arcsin\{\cos\bar{\theta}_c\cdot(-\frac{d\varepsilon_N}{d\gamma})\} + \mu$$

$$\fallingdotseq \lambda\cdot(-\frac{d\varepsilon_N}{d\gamma}) + \mu \qquad (18)$$

Substituting Eqs. (16) and (17) into Eq. (9), the relation between τ/σ_N and ε_N can be derived as follows.

$$\frac{\tau}{\sigma_N} = \lambda\cdot\arccos\{\cos\bar{\theta}_o\cdot(1+\varepsilon_N)\} + \mu$$

$$\fallingdotseq \lambda\cdot\sqrt{\bar{\theta}_o^2 - 2\varepsilon_N} + \mu \qquad (19)$$

$$\frac{\tau}{\sigma_N} = \lambda\cdot\arccos\{2\cos\bar{\theta}_p - \cos\bar{\theta}_o\cdot(1+\varepsilon_N)\} + \mu \qquad (20)$$

On the assumption that the direction of the principal stress coincides with that of the principal strain increment, the relationship between the principal stress ratio (σ_1/σ_3) and the principal strain increment ratio ($d\varepsilon_3/d\varepsilon_1$) is derived from Eq. (18) as follows.

$$\frac{d\varepsilon_3}{d\varepsilon_1} = \frac{\sigma_1/\sigma_3 - 2\mu\cdot\sqrt{\sigma_1/\sigma_3} + (\lambda-1)}{(1-\lambda)\cdot\sigma_1/\sigma_3 - 2\mu\sqrt{\sigma_1/\sigma_3} - 1} \qquad (21)$$

Now we try to derive a practical stress-strain relation. From Eq. (16) ε_N can be approximately described as follows by expanding $\cos\bar{\theta}$ in a series and neglecting the higher-order terms.

$$\varepsilon_N = (\cos\bar{\theta} - \cos\bar{\theta}_o)/\cos\bar{\theta}_o$$

$$\fallingdotseq \tfrac{1}{2}(\bar{\theta}_o^2 - \bar{\theta}^2)/(1 - \tfrac{1}{2}\bar{\theta}_o^2)$$

$$\fallingdotseq \tfrac{1}{2}(\bar{\theta}_o^2 - \bar{\theta}^2) = \tfrac{1}{2}(\bar{\theta}_o + \bar{\theta})\cdot(\bar{\theta}_o - \bar{\theta})$$

Since it may be assumed as $d\gamma = d\bar{\theta}$, we can assume that $(\bar{\theta}_o + \bar{\theta})/2$ is approximately equal to as far as $\bar{\theta}_o \fallingdotseq \bar{\theta}o$ (or $\varepsilon_N \fallingdotseq 0$). Substituting the above equation and the relation $\gamma \fallingdotseq (\bar{\theta}_o+\bar{\theta})/2$ into Eq. (9), we obtain:

$$\frac{\tau}{\sigma_N} = \lambda\cdot\bar{\theta} + \mu = \lambda\cdot(-\varepsilon_N/\gamma) + \lambda\cdot\bar{\theta}_o + \mu$$

$$= \lambda\cdot(-\varepsilon_N/\gamma) + \mu' \qquad (22)$$

where $\mu' = \lambda\cdot\bar{\theta}o + \mu$. Substituting Eq. (22) into Eq. (18) and integrating, we get:

$$\frac{\tau}{\sigma_N} = (\mu' - \mu)\cdot\log_e\frac{\gamma}{\gamma_o} + \mu \qquad (23)$$

$$\varepsilon_N = \frac{\mu - \mu'}{\lambda}\cdot\gamma\cdot[\log_e\frac{\gamma}{\gamma_o} - 1] \qquad (24)$$

γ_o is γ at the maximum compression point of ε_N where $d\varepsilon_N/d\gamma = 0$. From Eq. (23),

$$\frac{\tau}{\mu\cdot\sigma_N} = (\frac{\mu'}{\mu} - 1)\cdot\log_e\frac{\gamma}{\gamma_o} + 1 \qquad (25)$$

Therefore, the relationship of $\tau/\mu\sigma_N$ and γ/γ_o is represented by a straight line passing through the point (1, 1) on the semi-logarithmic paper. On the same assumption as that used in Eq. (21), the following relations can be derived from Eqs. (23) and (24) by applying an approximate operation.

$$\varepsilon_1 = \frac{\gamma_o\exp(-\frac{\mu}{\mu'-\mu})}{2}\cdot\exp[\frac{X}{2(\mu'-\mu)}]$$

$$\cdot[\frac{X^2}{8} + (\frac{1}{2} - \frac{1}{\lambda} - \frac{\mu'-\mu}{2})\cdot X + (\mu'-\mu)^2 - (\mu'-\mu) + \frac{2\mu'}{\lambda} + 1] \qquad (26)$$

$$\varepsilon_3 = \frac{\gamma_o\exp(-\frac{\mu}{\mu'-\mu})}{2}\cdot\exp[\frac{X}{2(\mu'-\mu)}]$$

$$\cdot[-\frac{X^2}{8} + (\frac{1}{2} - \frac{1}{\lambda} + \frac{\mu'-\mu}{2})\cdot X - (\mu'-\mu)^2 - (\mu'-\mu) + \frac{2\mu'}{\lambda} - 1] \qquad (27)$$

where $X = \sqrt{\sigma_1/\sigma_3} - \sqrt{\sigma_3/\sigma_1}$

COMPARISON WITH EXPERIMENTAL RESULTS

One of the experimental results obtained by simple shear tests (N.G.I. type) of Toyoura sand is shown in Fig. 6. In this figure, the gradient of the straight line up to the peak strength is 1.4~1.5 and the value at its intersection with the ordinate is 0.45, which is nearly equal to the frictional coefficient given by Rowe (1962). So these values agree very well with the theoretical relation given by Eq. (18). Furthermore, it is confirmed by experiments that Eq. (18) is applicable even to the tests of sands, in which σ_N is increased or decreased during shear, and also applicable to repetitious shear tests. This suggests that this relation may be independent of stress path.

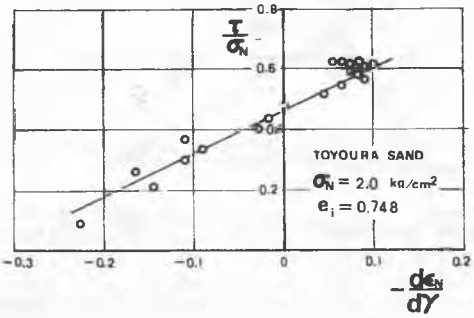

Fig. 6 Relationship between τ/σ_N and $d\varepsilon_N/d\gamma$ obtained by simple shear test

Now it may be supposed that the above-mentioned shearing mechanism for granular soils can be also applied to clays as far as clay aggregates behave as like as sand grains. Fig. 7 shows the experimental relationship of a normally consolidated clay between τ/σ_N and $d\varepsilon_N/d\gamma$ on the $(\tau/\sigma_N)_{max}$-plane, obtained by the drained triaxial test (the mean principal stress σ_m=p =1.0 kg/cm^2). The gradient of the straight line 1.2 corresponds to λ in Eq. (18), but

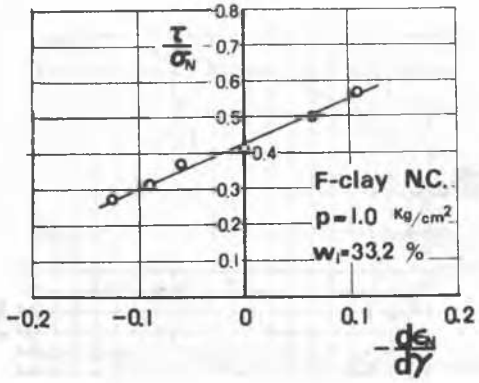

Fig. 7 Relationship between τ/σ_N and $d\varepsilon_N/d\gamma$ on the $(\tau/\sigma_N)_{max}$-plane obtained by triaxial test (Fujinomori clay)

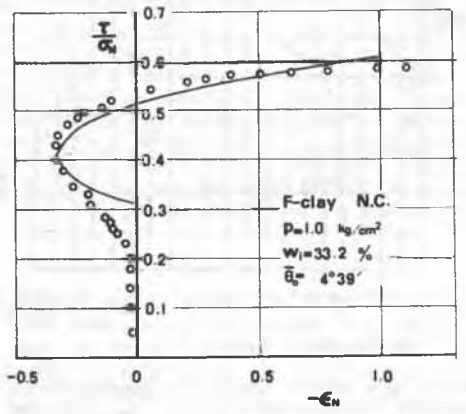

Fig. 8 Relationship between τ/σ_N and ε_N on the $(\tau/\sigma_N)_{max}$-plane obtained by triaxial test (Fujinomori clay)

it is a little smaller than the value obtained in Eq. (9) in the case of triaxial tests. This may be caused by the existence of the wedge-shaped zone left non-deformed near the cap and pedestal in a triaxial apparatus. In Fig. 8 the calculated curve from Eq. (19) almost coincides with the experimental values plotted from the same data used in Fig. 7. In Fig. 9 the relationship between σ_1/σ_3 and $d\varepsilon_3/d\varepsilon_1$ obtained by the drained triaxial test of Ishii River sand is plotted. The calculated curve in Fig. 9 is given by Eq. (21) using $\lambda = 1.2$ (in the case of triaxial tests) and the measured frictional coefficient between grains $\mu = 0.62$. This agrees very well with the experimental values. According to Rowe's stress-dilatancy theory, the theoretical values is a straight line passing through the origin, so it may be difficult to explain this data at least. Now, an example to verify Eq. (22) is shown in Fig. 10. This is a result of the drained triaxial test (σ_m=2.0 kg/cm², e_i=0.793; initial void ratio) of Ishii River sand. In Fig. 10 the axial strain, where the points begin to lie on the straight

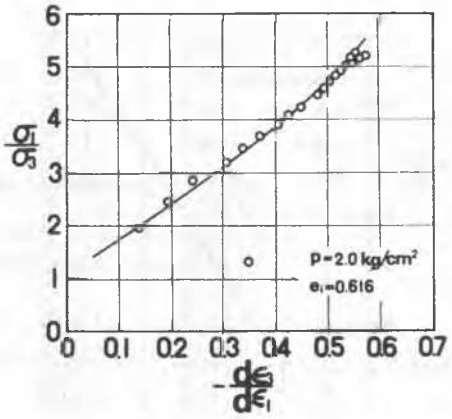

Fig. 9 Relationship between σ_1/σ_3 and $d\varepsilon_3/d\varepsilon_1$ (Ishii River sand)

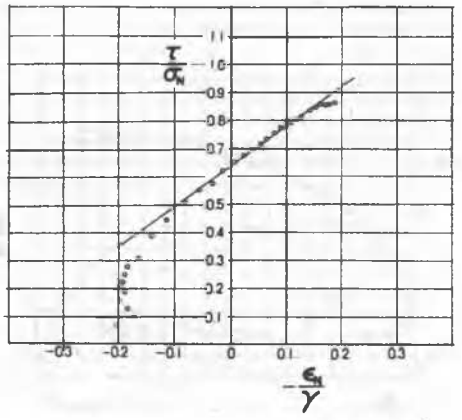

Fig. 10 Relationship between τ/σ_N and ε_N/γ (Ishii River sand)

line, is about 1~2%, so it may be approximately admitted that the main part up to the peak strength lies on the straight line. Similar results were obtained in the case of clays too. Fig. 11 shows the relation of Eq. (25) obtained by Ishii River sand under the following conditions; σ_m=2 kg/cm², σ_3=1 kg/cm², σ_3=2 kg/cm² and e_i=0.616~0.793. Such good results have been also obtained by other sands, clays and glass beads. Figs. 12 and 13 show the relationships obtained by Eqs. (23), (24), (26) and (27) in the cases of Ishii River sand and Fujinomori clay respectively under the conditions; σ_3=1 kg/cm², e_i=0.706 in Fig. 12 and σ_m=1 kg/cm², N.C. clay in Fig. 13. In all these figures the above-mentioned theory shows well agreement with experimental results.

CONCLUSIONS

The present stress-strain relations proposed should be essentially applied to the shearing behavior of soils in the drained condition, so it might be necessary in the case of the general stress condition to combine these relations

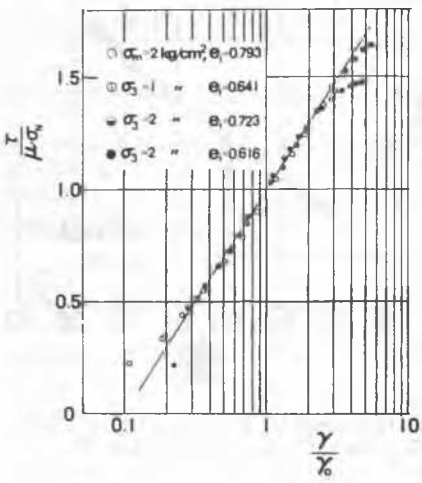

Fig. 11 Relationship between $\tau/\mu\sigma_N$ and γ/γ_o (Ishii River sand)

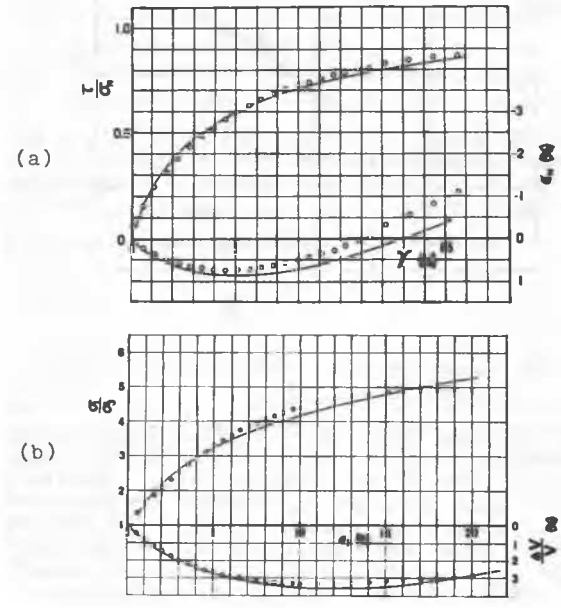

Fig. 12 Relationships among τ/σ_N, γ and ε_N (a) and among σ_1/σ_3, ε_1 and $\Delta V/V$ (b) (Ishii River sand)

with the relation of the consolidation phenomena. Among the coefficients of these equations such as λ, μ, μ', γ_o and $\bar{\theta}_o$, λ and μ are considered to be constants, $\mu'=\lambda\cdot\bar{\theta}_o+\mu$ and γ_o is related to $\bar{\theta}_o$, so in order to predict the general stress-strain relations under shear, it becomes important to decide the value of γ_o.

ACKNOWLEDGEMENT

The authors wish to thank Prof. T. Shibata of Kyoto University, Assist. Prof. D. Karube of Kobe University and Mr. F. Tatsuoka of Tokyo University for their helpful suggestion. Some experimental data given by Mr. H. Miyoshi and Mr. K. Asai are appreciated.

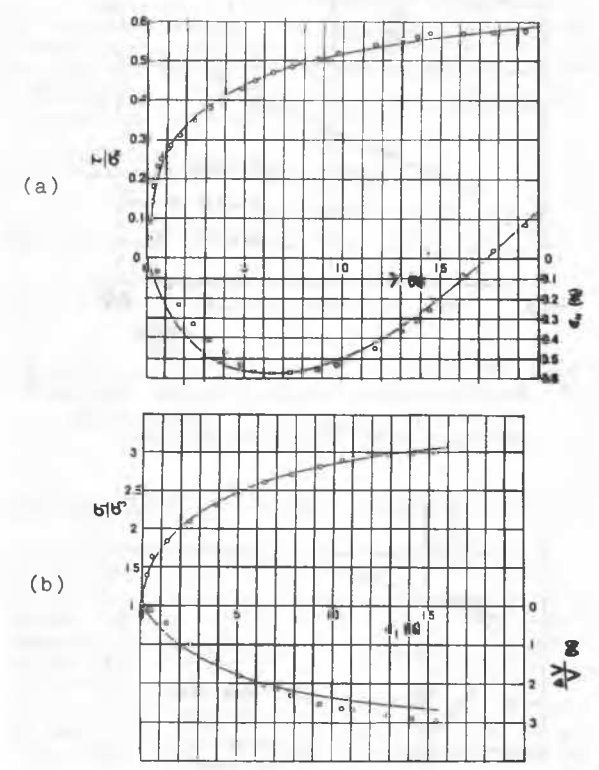

Fig. 13 Relationships among τ/σ_N, γ and ε_N (a) and among σ_1/σ_3, ε_1 and $\Delta V/V$ (b) (Fujinomori clay)

REFERENCE

Rowe, P.W.(1962): The Stress-dilatancy Relation for Static Equilibrium of an Assembly of Particles in Contact, Proc. Roy. Soc. London, Ser.A, Vol.269, 500-527.